

Contents lists available at ScienceDirect

Journal of Alloys and Compounds

journal homepage: www.elsevier.com/locate/jalcom



Electrodeposition and superconductivity of rhenium-iron alloy films from water-in-salt electrolytes



B. Malekpouri, K. Ahammed, Q. Huang*

Department of Chemical and Biological Engineering, The University of Alabama, Tuscaloosa, AL 35487, USA

ARTICLE INFO

Article history: Received 15 February 2022 Received in revised form 11 April 2022 Accepted 15 April 2022 Available online 19 April 2022

Keywords: Electrodeposition ReFe alloy Superconductor Water-in-salt Electrolyte Amorphous superconductor

ABSTRACT

Electrochemical deposition of rhenium-iron alloy from water-in-salt electrolytes containing a super-high concentration of lithium chloride is investigated. Different techniques, including cyclic voltammetry, chronoamperometry, X-ray fluorescence, scanning electron microscope, X-Ray diffraction, and electrical measurements at cryogenic temperature are used to characterize the alloy electrochemical system and the deposited films. The catalytic effect of iron on rhenium deposition is observed, where the deposition rate of rhenium significantly increases in the presence of iron. Alloying rhenium with iron significantly inhibits the recrystallization of the as-deposited amorphous films. At the same time, it also greatly suppresses the superconductivity of rhenium.

© 2022 Elsevier B.V. All rights reserved.

1. Introduction

Re, a refractory metal in group VIIB of the periodic table, has distinguished properties such as high melting point, high hardness, high tensile strength, low friction coefficient, high creep-rupture strength, and excellent mechanical stability. These properties have enabled different applications of rhenium in various industries, including aircraft, aerospace, catalysis, electrical contacts, filaments and thermocouples, and biomedical devices [1–7]. Furthermore, rhenium does not have ductile-to-brittle transition due to its hexagonal close-packed (hcp) crystal structure, making it useful for mechanical parts operated at low temperatures [3]. In addition, Re is a superconductive metal with a critical temperature of 1.7 K in a bulk state [8]. The critical temperature, or the transition temperature, is the temperature below which the electrical resistance of a material drops to zero, or at which a material transitions to a superconducting state. The critical temperature of Re has been found to increase depending on the form of the metal and method of fabrication. For example, it increases to 2.7 K for powder rhenium [9], 2.8 K for Re films deposited with electron beam evaporation [10], 2.9 K with shear strain resulted from highpressure torsion [11], and to 6 K for Re films electroplated in multilayers forms with other metals such as copper, gold and palladium [12]. This critical temperature of electrodeposited rhenium is higher

than the boiling point of helium, i.e. 4.2 K, making it more useful for cryogenic electronic applications [12,13].

Many works have been done on the electrodeposition of Re and its alloys from conventional aqueous electrolytes [14–23]. Because of the very low overpotential of hydrogen evolution reaction on rhenium surface, Re electrodeposition has low faradic efficiency and often results in brittle films. Adding iron group metals, i.e. iron, cobalt, and nickel, to the solution improves the deposition rate of rhenium as well as the faradic efficiency [18,20,24].

Water-in-salt electrolyte, an electrolyte with a super high concentration of salt such as lithium chloride, has been used for electrodeposition of rhenium and its alloys [13,25-27]. Due to the complete disruption of hydrogen bond network in such electrolytes, proton transport is hindered and therefore the rapid hydrogen evolution reaction in acidic media is mitigated. In addition, due to the decrease in hydrogen formation during electrodeposition of rhenium from the water-in-salt electrolyte, crack-free rhenium films can be deposited. The as-deposited rhenium films is found to be amorphous with a superconducting critical temperature of 6 K [13]. In a recent work by De et al. [26] on the electrodeposition of rhenium-cobalt alloy from the water-in-salt electrolyte, the catalytic effect of cobalt on the electrodeposition of rhenium is also reported, consistent with observations in conventional electrolytes. Different compositions of Re-Co alloy are obtained at different applied potentials, and the superconducting critical temperature decreases from 5.8 K for pure rhenium to 4.6 K, 2.3 K and no T_c above 1.8 K for Re₉₁Co₉, Re₈₀Co₂₀ and Re₇₅Co₂₅, respectively.

^{*} Corresponding author.

E-mail address: qhuang@eng.ua.edu (Q. Huang).

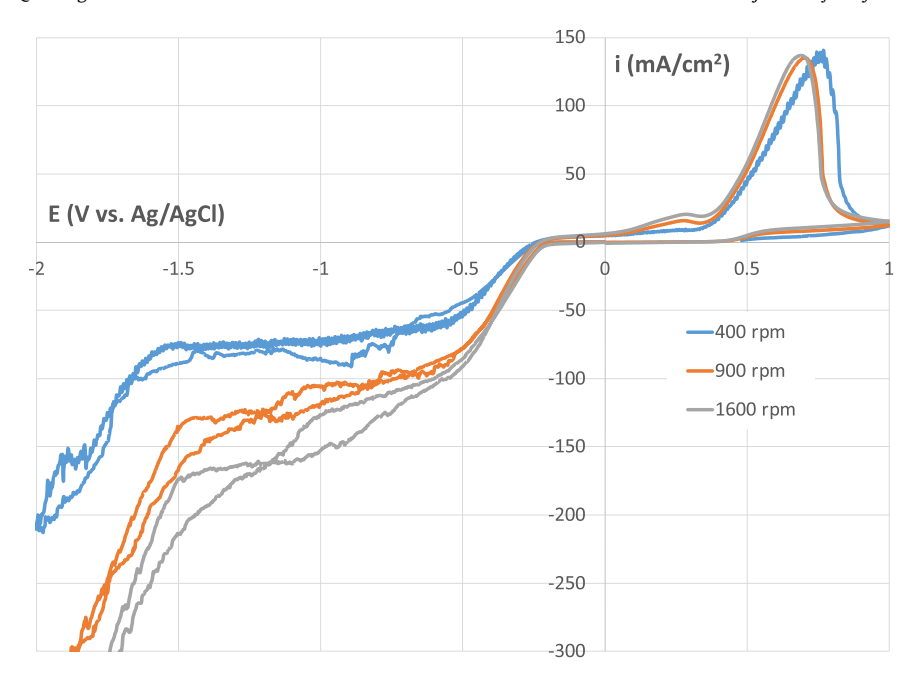


Fig. 1. CV studies at 20 mV/s at different rotation rates from a solution with a same composition containing 20 mM FeSO₄.

While the inclusion of ferromagnetic elements such as Co hinders the superconducting transition, ReFe alloy with a specific atomic ratio of 2:3 is expected to be a superconductor with an even higher $T_{\rm c}$ (than Re alone) of 6.5 K in its bulk form [8]. In this report, investigation is carried out on the electrodeposition of rhenium-iron alloy from waterin-salt electrolytes. The electrodeposition behaviors of elemental metal and alloys were determined. Film composition, surface morphology, crystal structure, and superconducting critical temperature are characterized and discussed along with each other.

2. Experimental

2.1. Electrochemical cell

An electrochemical cell with three compartments is used in this study. The anode is a platinum foil, placed in anolyte compartment separated from catholyte with a glass frit. Silver chloride (Ag/AgCl) electrode with saturated KCl is used as the reference, which is placed in the reference compartment connecting to the catholyte through a capillary. All the potentials reported in this paper are with reference to this Ag/AgCl. Three different substrates are used in this study. Platinum rotating disk electrode (RDE) is used for electrochemical studies, such as cyclic voltammetric (CV) and linear sweep voltammetry (LSV). Copper RDE is used for DC deposition to prepare films for characterization, such as thickness, composition, crystallographic structure, and surface morphology. Both RDEs have a diameter of 0.5 cm and a surface area of 0.196 cm². A third type of substrate, Si coupons with Au strip patterns, is used to deposit films for superconductivity measurement. The coupon is mounted onto a rotating electrode holder with Au strip facing down. The electrical contact is achieved with a spring-loaded contact pin on a patterned Au contact pad. The rotation rate during film deposition is fixed at 400 rpm, and it varies between 400 and 1600 rpm in the electrochemical studies.

2.2. Materials and chemical

A water-in-salt electrolyte containing 5 M LiCl, 100 mM H₂SO₄, and 25 mM ammonium perrhenate (NH₄ReO₄) is used for pure Re

deposition. The electrolytes used for alloy deposition contain various amounts of ferrous sulfate heptahydrate (FeSO₄·7H₂O). The concentration of FeSO₄ in the solution is varied from 1 to 50 mM for the different studies. All solutions are prepared using 18.2 M Ω ·cm deionized water and chemicals with at least ACS grade.

2.3. Instruments and procedures

An Autolab 302 N potentiostat is used for all electrochemical studies. The chronoamperometry method is used for DC deposition at different applied potentials. The scan rates in all CV and LSV analyses are fixed at 20 mV/sec. A Bruker M1 Mistral X-ray fluorescence spectroscope (XRF) with a 0.7 mm collimator and 50 kV is used to measure the thickness and composition of the deposited films. XRF measurements are conducted on five different spots on RDE surface, evenly distributed across the diameter, and the average of these five measurements is reported. The film compositions are reported using atomic percent, which are converted from weight percent used by XRF. A Thermo Fisher Apero Field Emission Scanning Electron Microscope (FE-SEM) is used to characterize the morphology of the deposited films. The crystal structure of the films is analyzed using a Bruker D8 power X-Ray Diffractometer (XRD) with Co K α source (wavelength = 1.79 Å), operated at 40 kV and 35 mA. XRD patterns are obtained for as deposited films as well as the films after annealing at three different temperatures, 200, 400, and 600 °C. A home built vacuum annealing chamber with a pressure below 0.1 mTorr is used for the annealing. An ultra-high pure nitrogen ambient is maintained during the cooling process after annealing. The superconducting critical temperature or transition temperature of the electrodeposited films is measured using a Quantum Design Dynacool Physical Property Measurement System (PPMS). This transition is determined by recording the film resistance along with temperature sweep from 30 K to 1.8 K. A four-probe configuration is used for the resistance measurement. Dupont 4929 N™ silver paint and aluminum wires are used to form four connections between the deposited film and the resistivity puck.

3. Results and discussion

3.1. Electrochemical study

Cyclic voltammetry (CV) studies are conducted to study the effects of rotation rate and iron concentration on ReFe alloy deposition. Fig. 1 shows the CVs at three different rotation rates in a same electrolyte containing 20 mM FeSO₄. Mass transport limited deposition currents are observed between –0.5 and –1.7 V for all three rotation rates from 400 to 1600 rpm. Higher rotation rate augments ion transport from the bulk solution towards the surface of working electrode, increasing the limiting current, as described in the Levich Equation below.

$$I_I = 0.62 \quad nFACD^{2/3} \nu^{-1/6} \omega^{1/2}$$
 (1)

where n is the number electrons transferred per ion, F is the Faraday's constant, A is the electrode surface area, C is the electrolyte concentration, D is the diffusion coefficient, ν is the kinematic viscosity, and ω is the angular velocity of the electrode. As a result, the limiting current increases for 1.5 and 2 times as the rotation rate increases for 2.25 and 4 times, following the relationship of square root. It will be discussed more later, but the integrated areas of anodic stripping peaks here do not reflect the amount of deposit during the cathodic scan because of the further reduction of the metal into soluble anion at highly negative potentials.

Fig. 2 shows a set of CV studies with different negative potential vertices. The anodic stripping region is kept the same to compare the amounts of deposit from the different cathodic deposition regions. The highest stripping peak is observed when the lower potential is –1.3 V, beyond which the amount of deposition decreases again. This decrease has been observed previously in pure Re deposition. The same phenomenon is also observed here in ReFe alloy deposition and is believed to result from a same mechanism, the further reduction of rhenium metal into rhenide anions. Among the different

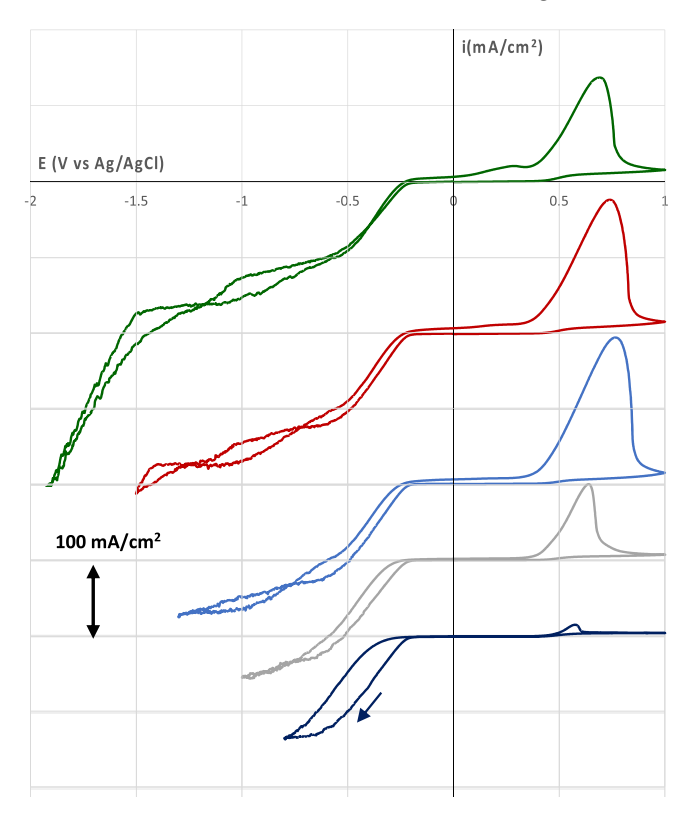


Fig. 2. CV curves *at 20 mV/s* with the different *lower* potentials *vertices at* rotation rate of 1600 rpm in a solution containing 20 mM FeSO₄.

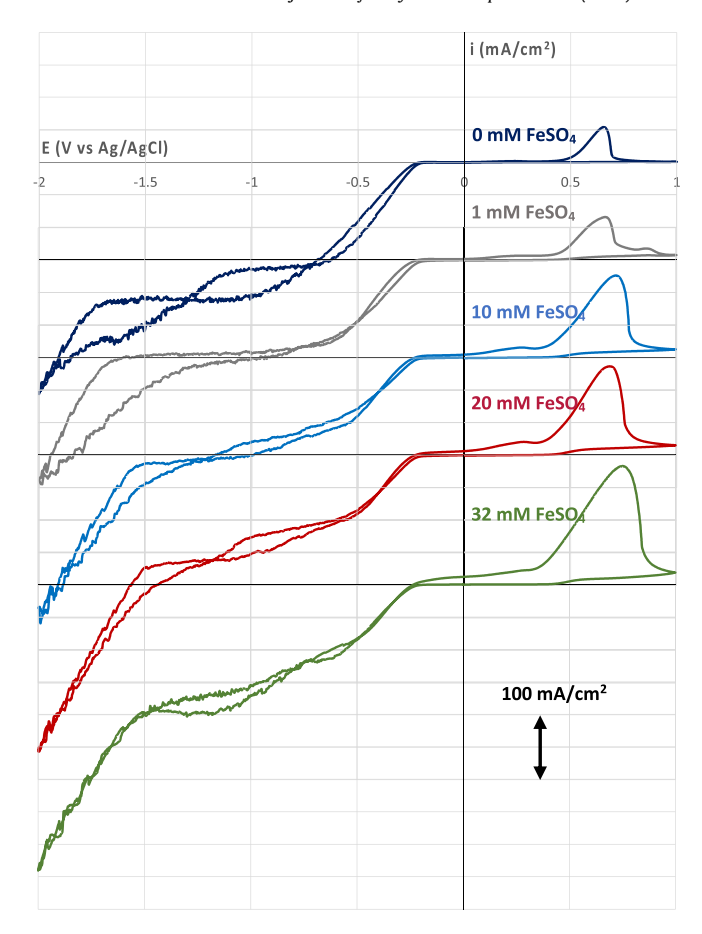


Fig. 3. CV studies $(20\,\text{mV/s})$ in solutions with different concentrations of FeSO₄ from 0 to 35 mM using a rotation rate of 1600 rpm.

cases, a pronounced hysteresis is observed in the cathodic CV when the vertex is at -0.8 V, where the current density is higher in the forward scan than the reverse scan. This suggests that the activity of hydrogen evolution reaction (HER) is higher on Pt than the electrode after the cathodic scan. Such strong hysteresis is not observed in pure Re deposition, and the presence of Fe in electrolyte is believed to play a role here. However, more study will be required to understand why this hysteresis is the most pronounced for that case and it gradually diminishes as the voltage sweeps to more negative vertices.

Fig. 3 shows the CV studies in solutions containing different concentrations of FeSO₄ between 0 (pure rhenium) to 35 mM. First, the anodic stripping peak increases along with the iron concentration in solution, suggesting that more metal gets deposited. Second, an impact on the cathodic current is also observed. A flat current plateau is evident in the pure Re electrolyte or with a minimum Fe concentration of 1 mM, reflecting the limiting current of HER. However, when the Fe concentration is above 10 mM, the current continues to gradually increase along with the cathodic potential and this increase becomes more pronounced as the Fe concentration further increases. In other words, additional Faraday processes on top of HER become more significant in these cases, and this observation appears to be consistent with the increase of anodic stripping charge. Furthermore, a shoulder anodic stripping peak at potential between 0 and +0.4V emerges as the iron concentration increases, indicative of the stripping of less noble Fe in the deposit.

In order to further investigate the alloy deposition behavior along different potentials, direct-current (DC) electrodeposition is carried out in these solutions with various concentrations of FeSO₄ from 0 to 35 mM. Films are electrodeposited at six different applied potentials

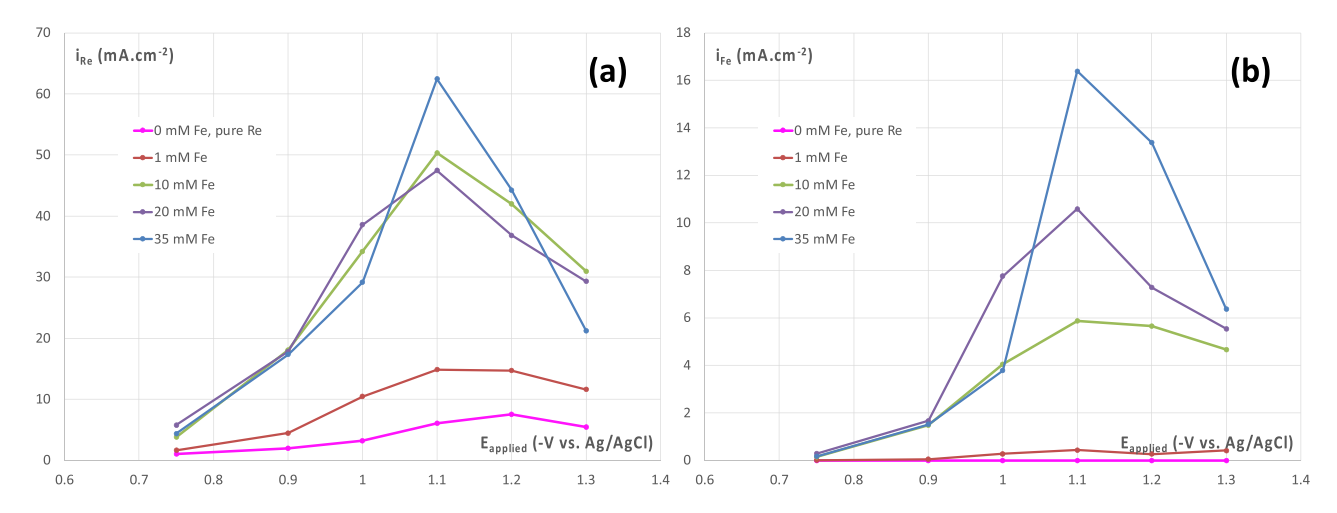


Fig. 4. Partial current density of (a) Re and (b) Fe during the electrodeposition of ReFe alloys at different constant potentials in electrolytes with various concentrations of FeSO4.

for various periods of time. The thickness and composition of the electrodeposited films are determined using XRF and are presented in Table S1 in Supplementary information. Fig. 4(a) and (b) show the partial current densities, or the deposition rates, of Re and Fe, respectively, calculated using Faraday's law. In pure Re electrolytes, with no Fe, the deposition current of Re reaches a maximum of about 8 mA/cm², consistent with previous studies [25]. Upon the addition of merely 1 mM Fe into the electrolyte, the rhenium partial current density more than doubled almost across all potentials studied. This enhancement of Re deposition rate by the presence of Fe is further magnified as the Fe concentration increases, reaching approximately 8 times increase in the presence of 35 mM FeSO₄. This clearly shows the strong catalytic effect of iron on the deposition rate of rhenium and is consistent with previous reports on rhenium alloy deposition from conventionally electrolytes using carboxylic acids as complexing agents [17,20,21].

Another observation worth noting is that Fe deposition rate increases as well at the same time, and this increase appears more pronounced than the Re deposition rate. For example, the max Re deposition rate at -1.1 V increases 4 times (from 15 to 62 mA/cm²) as the FeSO₄ concentration increases from 1 mM to 35 mM. But at the same time, the Fe deposition rate increases by 37 times, from 0.44 to 16.4 mA/cm². Closer look at the partial currents reveals some interesting observations. First, Re deposition rate before the maxima, i.e. at potentials more positive than -1.1 V increases with Fe concentration when the concentration is low. But when the Fe concentration reaches 10 mM, no further increase can be achieved suggesting a "saturation" of the enhancement effect on the Re deposition by Fe deposition. While the maximum Re deposition rate at -1.1 V sees further enhancement as Fe concentration increases from 10 to 35 mM, this difference is much minor compared with the difference between 1 and 10 mM. On the other hand, the partial current density of Fe deposition also follows a similar trend, namely. it is kinetic controlled before the maxima, depending on the applied potential rather than the Fe concentration. However, at a potential of -1.1 V. the maximum deposition rate of Fe approximately follows its concentration in solution, indicative of a mass transport controlled deposition rate. As the potential further decreases below -1.1 V, the partial current densities of both metals decrease, consistent with the discussion in Fig. 2, where less metal is deposited due to further reduction of Re into soluble rhenide anion.

The catalytic effect of Fe and other iron-group elements on Re deposition in conventional electrolyte with complexing agents was reported before and was explained with an electroless deposition mechanism of rhenium upon the oxidation of iron-group metals [20]. Here, we observe that the deposition of Fe in alloy largely

retains its elemental deposition behavior before the maxima, beyond which the loss of Fe deposit is believed to occur due to the disintegration of deposit upon the further reductive dissolution of Re.

3.2. Film morphology

The morphology of the electrodeposited films is characterized using FE-SEM. Fig. 5 shows the Re-Fe alloys electrodeposited at a DC potential between -0.9 V to -1.1 V from the solution containing 20 mM FeSO₄. All films under visual inspection are smooth and shiny with a silver color luster. As the applied potential becomes more negative than -1.2 V, darker films are deposited probably due to the inclusion of oxides or hydroxides of rhenium and iron. No cracks were observed on any of the films, consistent with our previous results on pure Re films [13,25]. Nodules with diameter up to a few microns can be observed on the films. Among them, the nodules are more uniform in size at -0.9 V, whereas greater difference or more polarized nodule sizes are observed as a more negative potential of -0.95 V is used. At -1 V, not only do these nodules remain dramatically different in size, but also additional small grains start to nucleate and grow on top of the large nodules, suggesting a much higher active nucleation sites at a more negative potential. Such small grains start to grow even earlier and become even more dominant as the potential reaches a more negative -1.1 V, resulting in the apparent cauliflower type of film morphology.

3.3. Crystallographic structure

XRD is used to characterize the crystallographic structures of electrodeposited films as well as the films after annealing at different temperatures. The results are presented in Fig. 6. In this set of studies, three duplicates of six alloy films with Fe content ranging from about 10 at% to about 60 at% are prepared on Cu RDEs at various potentials using two different alloy solutions with FeSO₄ concentrations at 20 and 50 mM. In addition, pure Re films are prepared from Re elemental electrolytes without FeSO₄ using a constant potential of -1 V. The time of deposition is also varied depending on the applied potential so that all the films in this set of studies are between 350 and 500 nm. Sides et al. [18] reported that electrodeposited pure Re films showed significant recrystallization upon annealing at 200 °C when the films are thicker than 300 nm whilst such grain growth was much alleviated when the film thickness falls to 200 nm or below. The control of film thickness between 350 and 500 nm in this study avoids any ambiguity due to thickness effect.

The three sets of duplicates are respectively annealed at three different temperatures. Fig. 6(a) shows the XRD patterns of seven as-

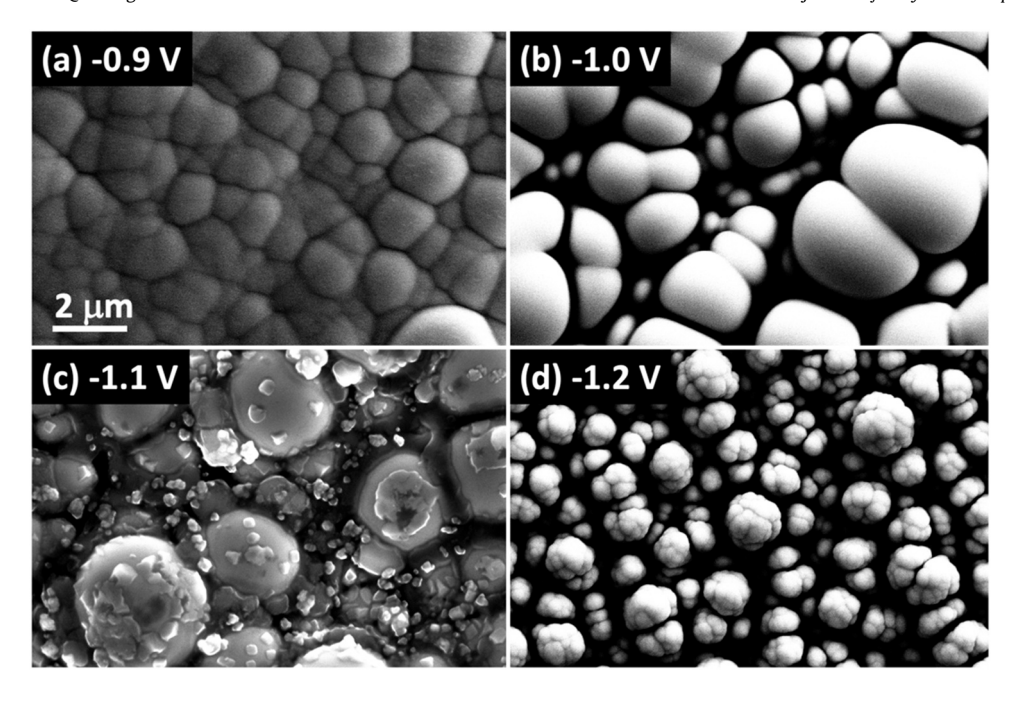


Fig. 5. Morphology of the deposited films obtained at different applied potentials.

deposited films, where only the peaks from copper substrates are observed. A broad background peak with 20 between 40° and 55° is also observed, indicative of the amorphous structure of all electrodeposited films regardless of composition. In the first annealing attempt, all seven films are annealed at 200 °C for 30 min, which has been previously reported as a suitable condition (enough temperature and time) for the recrystallization of pure rhenium [28]. As shown in Fig. 6(b), this condition has been confirmed here. Recrystallization is observed for the pure rhenium film, which presents a hcp structure with no apparent preferred crystal growth orientation. On the other hand, no recrystallization is observed for any of the alloy films. The presence of merely 10 at% Fe in the alloy effectively prevents the recrystallization at 200 °C. Fig. 6(c) shows the XRD pattern of films with similar composition annealed at 400 °C for 6 h. Upon Annealing at this higher temperature for a longer time, recrystallization is observed for three ReFe alloy films with up to 21 at% Fe. In comparing the XRD patterns with the pure Re case, these alloys with 10-20 at% showed a slightly preferred growth in the c-direction of a hexagonal lattice. For example, the (002) reflection is much stronger than (100) reflection for these alloys whilst it is the opposite for pure Re films. This preference in *c*-direction can also be found in other reflections such as the relative intensity between (110) and (103) reflections. In addition to this growth direction preference, there is also a shift of the peak positions due to the alloying. This drift increases with the Fe content in the alloy films. Alloy films with Fe content 32 at% and beyond remains amorphous upon this 400 °C with no Re peaks observed. Fig. 6(d) shows the XRD patterns of the third duplicate set after 600 °C annealing for 12 h. The observations discussed above for 400 °C annealing remains unchanged, except that the alloy film with 36 at% starts to recrystallize and some minor peaks emerge. However, the broad peak between 44° and 55° largely remains unchanged, suggesting the majority of film has not yet recrystallized and is still amorphous. This is more so for films with even higher Fe content, where no peaks are observed. Nevertheless, the right shift of peak position continues for the Re₆₄Fe₃₆ film, a result of decreasing lattice size.

As summarized from Fig. 6, it is evident that alloying with Fe prevents the recrystallization of Re despite the fact that Fe appears substitutional in all crystallized films having the intrinsic hcp structure of Re. This is quite unexpected as alloy films with up to

25 at% Co in our previous studies all readily recrystallize upon 200 °C annealing [26]. It is worthy noting that all ReFe films show hcp Re structures upon crystallization and no ReFe or Fe peaks are observed even for the films annealed at 600 °C for 12 h. This temperature appears not enough for the formation of new ReFe alloy phases such as P phase and σ phase [29]. Studies at even higher temperatures would be needed to form these phases while avoiding other complications such as interdiffusion with seed, thermal expansion mismatch, and film oxidation.

The positions of (100) and (002) peaks in Re and ReFe alloy films annealed at 600 C as well as the fitted lattice parameters, a and c, are summarized in Table 1. First, the fitted parameters of pure Re are a = 2.7552 Å and c = 4.4401 Å, consistent with the standard parameters of pure Re [30]. Upon the alloying of Fe, the lattice decreases in size in both a and c directions. This decrease continues as the Fe content in alloy increases. While this lattice contraction has also been reported for ReCo alloys [26], it is less pronounced in ReFe system. The atomic size of Fe is slightly larger than Co, which may relate to this difference in alloy lattice size.

It is not clear why the incorporation of small amount of Fe behaves completely differently from Co, significantly inhibiting the recrystallization of Re. While more detailed studies will be needed to further understand the mechanism, a brief discussion is provided below for some potential reasons. Because the atomic radius difference between Re and Fe is slightly smaller than Re and Co, Fe would be expected to be easier to be incorporated to a Re crystal. On the other hand, bulk Fe has a cubic structure, whilst Co has the same hcp structure as Re. More importantly, Fe has a limited solubility in Re and Co-Re are completely miscible [29,31]. These apparently contribute to the different effects of Fe and Co on the recrystallization of amorphous Re alloys. Another contribution may result from the different electronegativity of Fe and Co. While Re, Fe, and Co are all metals, which are not likely to exist as an anion, yet partial charge transfer may occur when they form alloys or bimetallic compounds [32]. In this case, Re is expected to be partially negative charged, and Fe and Co partially positive charged. This partial charge transfer is expected to be more pronounced in Fe-Re due to a greater difference in electronegativity than Co-Re. This difference may have also contributed to the inhibition in FeRe recrystallization.

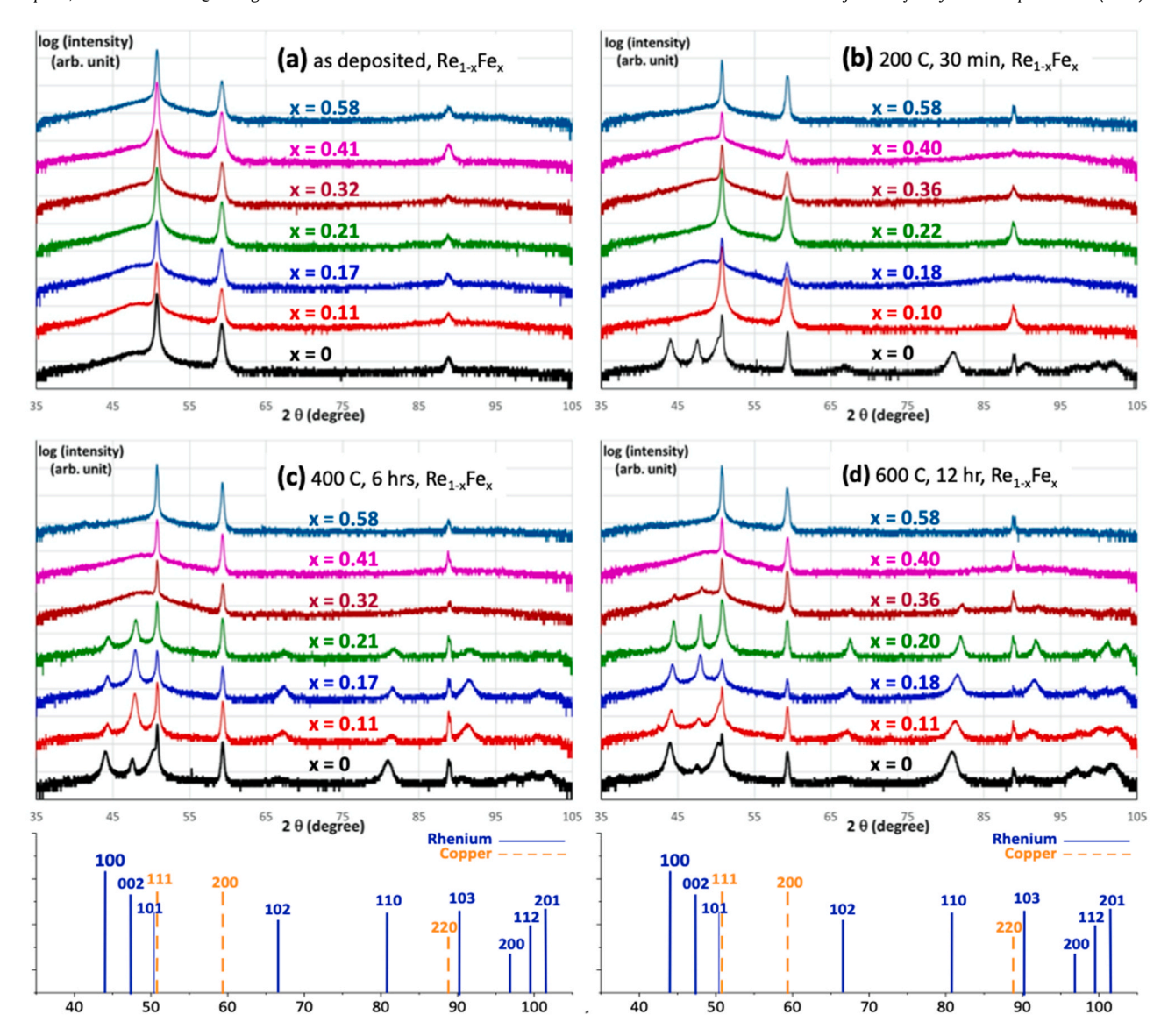


Fig. 6. XRD patterns of rhenium-iron alloy films (a) before annealing, after annealing at (b) 200 °C, (c) 400 °C (d) 600 °C. XRD standards of pure Re and Au are included in (c) and (d).

Table 1Lattice parameters of pure rhenium and ReFe alloys with different Fe contents.

Composition	Peak position (20)		Lattice parameters (Å)	
	(100)	(002)	а	с
Re (literature)			2.761	4.456
Re	44.035°	47.525°	2.7552	4.4401
Re ₈₉ Fe ₁₁	44.105°	47.605°	2.7520	4.4328
Re ₈₃ Fe ₁₇	44.240°	47.930°	2.7430	4.4040
Re ₇₉ Fe ₂₁	44.466°	47.986°	2.7298	4.3996
Re ₆₆ Fe ₃₆	44.595°	48.160°	2.7223	4.3847

3.4. Superconductivity

The superconducting critical temperature of ReFe alloy films is measured before annealing (as-deposited films). The sheet resistance of film is measured along a temperature sweep from 30 K to 1.8 K using the PPMS. Pure rhenium films and Re-Fe alloy films with different Fe contents are deposited on the Au strip patterns on silicon coupons at different potentials. All deposited films have a thickness between 240 and 440 nm measured with XRF. The sheet

resistance of all deposited films measured at room temperature are close, which also confirms the similar thickness of the films.

While bulk Re_2Fe_3 alloy prepared with arc-melting has been reported to show a T_c at 6.5 K [33], our electrodeposited ReFe alloy films with more than 30 at% Fe fail to recrystallize across the annealing conditions used in this study. On the other hand, none of the as deposited amorphous films with iron content between 6 to 60 at% shows any superconductivity down to 1.8 K, in other words, no superconducting transition is observed above 1.8 K. Alloying Re with a magnetic transition metal is expected to have a negative impact on superconductivity in general. For example, the T_c of amorphous ReCo alloy gradually decreases with increasing Co content and no superconductivity could be observed beyond 1.8 K for ReCo films containing over 20 at% Co [26]. However, in this study, a mere incorporation of 6 at% Fe completely suppresses the superconducting transition above 1.8 K.

In order to determine the critical Fe content for this suppression, different alloy films with even lower Fe contents from 1.4 to 5.5 at% are deposited from an electrolyte with a much lower FeSO $_4$ concentration of 1 mM. The deposition condition as well as the composition and thickness of these rhenium-iron alloy films are

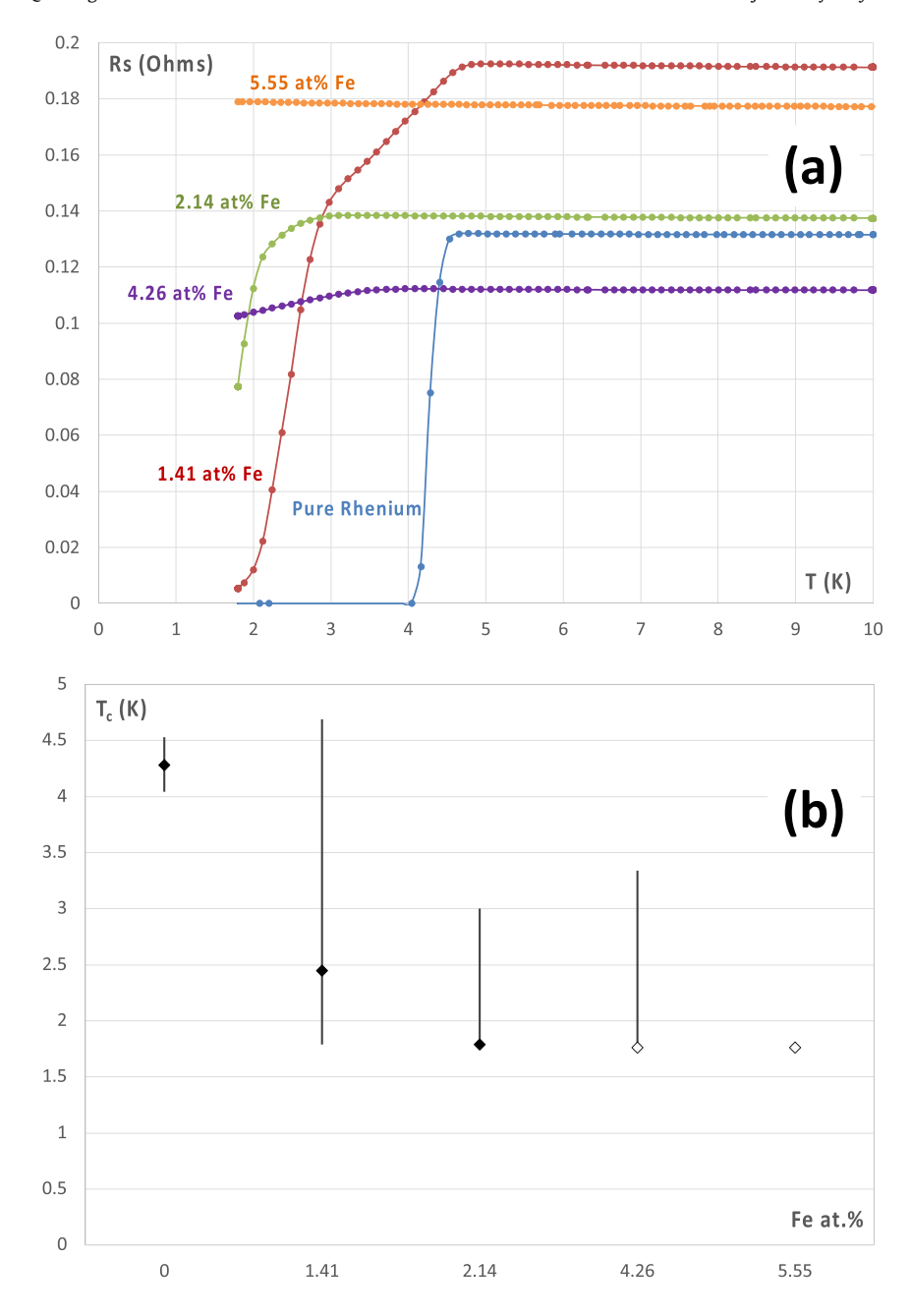


Fig. 7. (a) Resistance measurements along temperature sweep for pure Re and ReFe alloy films with different compositions between 1.4 and 5.5 at% Fe; and (b) the starting and ending temperature of the superconducting transition (solid line) as well the temperature at which the film resistance drops to half of the value before transition (solid diamond). Empty diamond represents 50% drop was not achieved above the temperature limit of PPMS.

summarized in Table S2 in Supplementary information. Pure Re is included in this set of studies for comparison The film resistance is measured along temperature sweep in PPMS and is plotted in Fig. 7(a). Fig. 7(b) is a plot in attempt to summarize the superconducting transition behaviors of alloy films with different composition by capturing the starting and ending temperature of transition as well as the temperature at which the film resistance drops to half of the value before transition. Pure Re film shows a transition at T_c of 4.6 K, slightly lower than our previous work probably due to a thickness effect [28]. In the case of 2.14 at% Fe, this transition is delayed to a lower T_c of at about 2.5 K, and this transition is barely completed down to 1.8 K, the lower limit of PPMS. For the alloy with a lower Fe content of 1.41 at%, two stages of transition are observed. The resistance starts to decrease slowly at a temperature of about 4.6 K, the same transition temperature of pure Re.

A second stage of transition starts at another temperature of about 3 K, where the resistance starts to drop much more rapidly. This may reflect a non-homogeneity of the Fe distribution in the alloy with such a low Fe content. Regions with purer Re starts the superconducting transition at 4.6 K, whilst the other regions with low but various Fe contents result in gradual transition below 4.6 K until the majority fraction of film with a slightly higher Fe content (than average) starts the transition at about 3 K. Such non-homogeneity effect has largely disappeared or is not evident anymore once the average Fe content becomes higher, beyond 2% in this case. The superconducting transition barely starts above 1.8 K at a higher Fe content of 4.26 at% and completely disappears at 5.5 at% Fe. In comparison with our early studies on rhenium-cobalt alloy films [26], a similar trend is evident for both alloys, where the critical temperature decreases with the increase of iron-group metal

content until the transition can no longer be observed above 1.8 K. On the other hand, superconductivity vanished at a much lower percent of the alloying element for Fe than Co, i.e. 6 at% Fe versus 25 at% Co. It has been reported that lattice expansion or tensile strain results in an enhanced critical temperature of Re [11,34] and the relaxation of lattice strains degrades such enhancement, i.e., the T_c falls back towards its intrinsic value [35]. However, between ReFe and ReCo cases, the latter has a much more pronounced decrease in lattice size while maintaining the superconductivity up to a much higher alloy content. On the other hand, bulk Fe metal has a much higher atomic magnetic moment than Co. While the detailed atomic moment depends on the host material and alloy composition and remains unknown, the stronger decrease of critical temperature in ReFe alloy is believed to result from the stronger atomic magnetic moment of Fe atoms.

4. Conclusion

Rhenium-iron alloy films with 1-60 at% Fe are successfully deposited using DC deposition at constant potentials. The rhenium deposition rate is significantly increased upon the addition of iron in electrolyte, where a 10-fold increase could be observed with 35 mM Fe. Nodular surface morphology is observed for the films deposited at lower potentials whilst finer grains on top of nodules and eventually cauliflower morphology are observed at more negative potentials. XRD studies clearly show that alloying Re with Fe hinders the recrystallization of Re. While pure Re recrystallizes at 200 °C, no recrystallization is observed in any of rhenium-iron alloy at this temperature. In addition, the inclusion of 30 and 40 at% Fe is enough to completely inhibit Re recrystallization at 400 °C and 600 °C, respectively. For those alloys with recrystallization at lower Fe contents, hcp structure native to pure Re is observed. The superconducting critical temperature of film decreased from 4.6 K for Pure Re to 3 and 2.7 K for alloys with merely 1 at% and 2 at% Fe, respectively. No superconducting transition could be observed beyond 1.8 K for Re-Fe alloy films with more than 6 at% Fe.

CRediT authorship contribution statement

B. Malekpouri: Data curation, Investigation, Formal analysis, Writing - original draft. K. Ahammed: Data curation, Investigation, Writing - review & editing. Q. Huang: Conceptualization, Formal analysis, Writing - original draft, Writing - review & editing.

Declaration of Competing Interest

The authors declare the following financial interests/personal relationships which may be considered as potential competing interests: Qiang Huang reports financial support was provided by National Science Foundation.

Acknowledgements

This work is supported by National Science Foundation through grants 1662332, 1921840 and 2016541. The Alabama Analytical Research Center at the University of Alabama is acknowledged for the access and training of equipment for material characterization.

Appendix A. Supporting information

Supplementary data associated with this article can be found in the online version at doi:10.1016/j.jallcom.2022.165077.

References

[1] J.J. Diaz, Pure rhenium metal, IEEE Potentials 15 (1) (1996) 37.

- [2] I.R. Davis, P. Allen, S. Lampman, T.B. Zorc, S.D. Henry, J.L. Daquila, A.W. Ronke, Metals Handbook: Properties and Selection: Nonferrous Alloys and Specialpurpose Materials, ASM international, 1990.
- A. Naor, N. Eliaz, E. Gileadi, S.R. Taylor, Properties and applications of rhenium and its alloys, AMMTIAC Q. 5 (2010) 11.
- [4] T. Thevenin, L. Arles, M. Boivineau, J. Vermeulen, Thermophysical properties of
- rhenium, Int. J. Thermophys. 14 (3) (1993) 441. C.T. Sims, C.M. Craighead, R.I. Jaffee, Physical and mechanical properties of rhenium, JOM 7 (1) (1955) 168.
- [6] J. Biaglow. High temperature rhenium material properties. in 34th AIAA/ASME/SAE/ ASEE Joint Propulsion Conference and Exhibit, 3354, 1998.
- J. Biaglow. Rhenium material properties. in 31st Joint Propulsion Conference and Exhibit, 2398, 1995.
- W.M. Haynes, CRC handbook of chemistry and physics. 96th ed. 2015, Boca Raton, FL: CRC press.
- J. Hulm, B.B. Goodman, Superconducting properties of rhenium, ruthenium, and osmium, Phys. Rev. 106 (4) (1957) 659.
- [10] A.U. Haq, O. Meyer, Electrical and superconducting properties of rhenium thin films, Thin Solid Films 94 (2) (1982) 119.
- [11] M. Mito, H. Matsui, K. Tsuruta, T. Yamaguchi, K. Nakamura, H. Deguchi, N. Shirakawa, H. Adachi, T. Yamasaki, H. Iwaoka, Large enhancement of superconducting transition temperature in single-element superconducting rhenium by shear strain, Sci. Rep. 6 (2016) 36337.
- [12] D.P. Pappas, D.E. David, R.E. Lake, M. Bal, R.B. Goldfarb, D.A. Hite, E. Kim, H.-S. Ku, J.L. Long, C.R.H. McRae, L.D. Pappas, A. Roshko, J.G. Wen, B.L.T. Plourde, I. Arslan, X. Wu, Enhanced superconducting transition temperature in electroplated rhenium, Appl. Phys. Lett. 112 (18) (2018) 182601.
- [13] Q. Huang, Y. Hu, Electrodeposition of superconducting rhenium with water-insalt electrolyte, J. Electrochem. Soc. 165 (16) (2018) D796.
- [14] L. Netherton, M. Holt, Electrodeposition of rhenium-nickel alloys, J. Electrochem. Soc. 98 (3) (1951) 106.
- [15] L. Netherton, M. Holt, Electrodeposition of rhenium-cobalt and rhenium-iron alloys, J. Electrochem. Soc. 99 (2) (1952) 44.
- [16] R. Schrebler, M. Merino, P. Cury, M. Romo, R. Cordova, H. Gomez, E. Dalchiele, Electrodeposition of Cu-Re alloy thin films, Thin Solid films 388 (1-2) (2001)
- [17] N. Eliaz, E. Gileadi, Induced codeposition of alloys of tungsten, molybdenum and rhenium with transition metals, in: C.G. Vayenas, R.E. White, M.E. Gamboa-Aldeco (Eds.), Modern Aspects of Electrochemistry, Springer New York, New York, NY, 2008, p. 191.
- [18] A. Naor, N. Eliaz, E. Gileadi, Electrodeposition of rhenium-nickel alloys from aqueous solutions, Electrochim. Acta 54 (25) (2009) 6028.
- [19] B.P. Hahn, K.J. Stevenson, Electrochemical synthesis and characterization of mixed molybdenum-rhenium oxides, Electrochim. Acta 55 (22) (2010) 6917.
- [20] A. Naor, N. Eliaz, L. Burstein, E. Gileadi, Direct experimental support for the catalytic effect of iron-group metals on electrodeposition of rhenium, Electrochem. Solid-State Lett. 13 (12) (2010) D91.
- [21] A. Naor, N. Eliaz, E. Gileadi, Electrodeposition of alloys of rhenium with irongroup metals from aqueous solutions, J. Electrochem. Soc. 157 (7) (2010) D422.
- [22] M.C. Sagiv, N. Eliaz, E. Gileadi, Incorporation of iridium into electrodeposited rhenium-nickel alloys, Electrochim. Acta 88 (2013) 240.
- [23] H. Cao, D. Chai, L. Wu, G. Zheng, Communication-A mechanistic study on electrodeposition of rhenium from acidic solution of ammonium perrhenate, J. Electrochem. Soc. 164 (13) (2017) D825.
- [24] F. Contu, S. Taylor, Further insight into the mechanism of Re-Ni electrodeposition from concentrated aqueous citrate baths, Electrochim. Acta 70 (2012) 34.
- Q. Huang, T.W. Lyons, Electrodeposition of rhenium with suppressed hydrogen evolution from water-in-salt electrolyte, Electrochem. Commun. 93 (2018) 53.
- [26] S. De, W.D. Sides, T. Brusuelas, Q. Huang, Electrodeposition of superconducting rhenium-cobalt alloys from water-in-salt electrolytes, J. Electroanal. Chem. 860 (2020) 113889.
- [27] S. De, J. White, T. Brusuelas, C. Patton, A. Koh, Q. Huang, Electrochemical behavior of protons and cupric ions in water in salt electrolytes, Electrochim. Acta 338 (2020) 135852.
- [28] W.D. Sides, E. Hassani, D.P. Pappas, Y. Hu, T.-S. Oh, Q. Huang, Grain growth and superconductivity of rhenium electrodeposited from water-in-salt electrolytes, J. Appl. Phys. 127 (8) (2020) 085301.
- [29] A. Breidi, M. Andasmas, J. Crivello, N. Dupin, J. Joubert, Experimental and computed phase diagrams of the Fe-Re system, J. Phys.: Condens. Matter 26 (48) (2014) 485402.
- [30] P. Villars, L. Calvert, Pearson's Handbook of Crystallographic Data for Intermediate Phases, American Society of Metals, Cleveland, OH, 1985.
- [31] T.B. Massalski, H. Okamoto, P. Subramanian, L. Kacprzak, W.W. Scott, Binary Alloy Phase Diagrams, American Society for Metals, Metals Park, OH, 1986.
- [32] J. Rodriguez, Physical and chemical properties of bimetallic surfaces, Surf. Sci. Rep. 24 (7–8) (1996) 223.
- [33] E. Savitskii and O.K. Khamidov, Superconducting Metallic Compounds of Rhenium, Proceedings of the IV All-Union Coference on Physical Chemistry, Metal Science. and Metal Physics - Superconductors (trudy IV Vsesoi u iznogo soveshchanii a po fiziko-khimii, metallovedenii u i metallofizike - sverkhprovodnikov), 1969, 5. 3.
- [34] O. Zhu, G. Xiao, Y. Cui, W. Yang, S. Wu, G.-H. Cao, Z. Ren, Anisotropic lattice expansion and enhancement of superconductivity induced by interstitial carbon doping in rhenium, J. Alloy. Compd. 878 (2021) 160290.
- C. Chu, T. Smith, W. Gardner, Superconductivity of rhenium and some rheniumosmium alloys at high pressure, Phys. Rev. Lett. 20 (5) (1968) 198.